Title:

Cryptic Evolution of Heteroresistance as Adaptation to Treatment Interruptions

Authors: Muqing Ma [1,2], Tai do [1], and Minsu Kim [1,2,3] *

[1] Department of Physics, Emory University, Atlanta, GA, 30322. U.S.A.

[2]Antibiotic Resistance Center, Emory University, Atlanta, GA, 30322. U.S.A

[3] Graduate Division of Biological and Biomedical Sciences, Emory University, Atlanta, GA, 30322. U.S.A.

* To whom correspondence should be addressed. Tel: 404-727-8037; FAX: 404-727-0873; Email: minsu.kim@emory.edu

Abstract

The evolution of antibiotic resistance is traditionally understood as a selective sweep to fixation, yielding easily detectable, population-wide resistance. Many clinical isolates, however, exhibit a subtle phenotype in which resistance remains masked within a susceptible majority despite a clonal genetic background: a phenomenon clinically recognized as heteroresistance (HR). Treatment failure driven by such heterogeneous phenotype has been widely reported across bacterial and fungal infections and in cancer therapy. To understand when, how, and why HR evolves, we experimentally evolved HR de novo from susceptible *Escherichia coli* and defined its genetic and fitness basis. Prolonged gaps in antibiotic exposure are required for HR to evolve, implicating treatment interruptions as a key driver. HR emerges rapidly and reproducibly with minimal antibiotic use, yet its emergence is not readily detected by routine susceptibility testing.

Single-cell fitness analyses reveal that an evolved HR strain dynamically organizes multiple phenotypic states with distinct growth–resistance trade-offs, enriching resistant cells during antibiotic exposure while allowing fast-growing susceptible cells to dominate during treatment interruptions. This contrasts with classical resistance, which carries a constitutive fitness cost. Despite this dynamic heterogeneity, single mutations are sufficient to generate HR, indicating a low evolutionary barrier. Notably, clinical isolates exhibited genetic and fitness signatures similar to our evolved strains, indicating shared selective pressures. Quantitative fitness modeling recapitulates the phase boundary between HR and classical resistance evolution, supporting the selective basis uncovered by our experiments. Together, our results establish HR as a readily evolvable resistance that leverages phenotypic flexibility to maximize survival while minimizing fitness costs, providing mechanistic insight into its emergence and prevalence.

Introduction

Antibiotic resistance is one of the most urgent threats to global health, undermining the efficacy of life-saving treatments. Infections that were once easily cured are becoming increasingly difficult to manage, leading to higher mortality rates, prolonged illness, long-term health complications, and rising healthcare costs.

The canonical model of resistance evolution is well established [1]. Antibiotic exposure eliminates susceptible cells, whereas cells that acquire resistance mutations or genes survive, transmit these determinants stably to their progeny, and expand clonally. As a result of this selective sweep, these genetic determinants are uniformly shared across the population. Owing to this uniformity, the resistance of the entire population is summarized by a single metric—the minimum inhibitory concentration (MIC) [2]. Based on the MIC-based testing, resistance is framed as a binary trait: an isolate either exhibits it or does not.

Yet growing evidence reveals a limitation of this paradigm. Many clinical isolates are neither fully resistant nor fully susceptible; instead, resistance stably coexists with susceptible cells within a clonal population: a phenomenon clinically recognized as heteroresistance (HR) [3,4]. A major challenge is that such isolates are not readily recognized by routine diagnostic tests yet still give rise to treatment failure, creating a discrepancy between diagnosis and therapeutic outcome.

HR was reported as early as the 1940s, during the early antibiotic era [5,6] and has since been observed across diverse bacterial species and antibiotic classes [7]. Epidemiological surveys report that the incidence of HR has increased steadily with antibiotic use [8]. In some settings, HR surpassed classical resistance as the predominant form of drug resistance [9]. Analogous forms of

HR and associated treatment failures have also been reported in fungal pathogens and cancer cells [10,11].

Despite its widespread clinical presence, the evolutionary origin of HR remains poorly understood. Antibiotic landscapes in clinical settings are complex, complicating efforts to identify the selective determinants that favor HR. Although one study reported the evolution of bet-hedging [12], a subsequent analysis showed the underlying phenotypic bifurcation was already present in the background strain [13]. More broadly, the de novo evolution of stochastic phenotypic switching is generally considered challenging as various environmental constraints and fitness trade-offs severely restrict the relevant parameter regime [14,15]. Moreover, one proposed mechanism of HR involves transient gene duplication arising as byproducts of DNA replication [16], which suggests that HR is intrinsic and preexisting. This view, however, is difficult to reconcile with epidemiological evidence showing a steady increase in HR incidence with antibiotic use [8].

To address this knowledge gap, we performed de novo evolution experiments beginning with a fully susceptible *Escherichia coli* K-12 strain. By systematically varying antibiotic exposure regimes, we evolved both HR and classical (population-wide) resistance, thereby defining the contrasting selective environments. HR evolution was cryptic yet rapid and reproducible, underscoring a major diagnostic blind spot. Whole-genome sequencing and genetic reconstruction identified the underlying mutations. Leveraging the unique opportunity to derive both HR and classical resistance from the same ancestral background, we performed direct head-to-head fitness comparisons at the population and single-cell resolution. The results revealed the adaptive basis of HR that exploits phenotypic flexibility to maximize growth and survival, in contrast to classical resistance which is genetically locked into fixed fitness costs. We also

discovered that clinical HR isolates exhibited genetic and fitness signatures similar to those of laboratory-evolved strains, indicating shared selective pressures. Finally, quantitative modeling unifies these findings into a predictive framework that accounts for the evolutionary divergence between HR and classical resistance. Our findings provide fundamental insights into when and how HR emerges and why it is prevalent.

Results

De novo evolution of antibiotic resistance

Colistin is a critical last-line antibiotic for treating multidrug-resistant Gram-negative infections when few alternatives remain. Colistin-HR and associated antibiotic failure were first described in clinical isolates of *Enterobacter cloacae* [17] and have been reported in a wide range of Gram-negative pathogens (Supplementary Table 1). Recent survey indicates that HR surpassed classical resistance as the predominant form of colistin resistance [9]. We used colistin as a model antibiotic to investigate the evolutionary principles of HR. To assess whether our findings extend beyond colistin, we further repeated the evolution experiments using the β-lactam antibiotic meropenem.

Although HR isolates have been frequently found clinically, their genetic backgrounds are poorly defined, their evolutionary ancestors and intermediate states are unavailable, and their selective histories remain unknown. To directly examine how bacteria evolve to acquire HR de novo, we therefore performed controlled evolution experiments using *Escherichia coli* K-12, a genetically well-characterized and experimentally tractable model system.

In routine clinical microbiology, antibiotic susceptibility is most commonly assessed using inhibition-zone-based assays such as disk diffusion (Kirby–Bauer) and gradient diffusion (Etest)

[18]. Etest and disk diffusion performed on the ancestral *E. coli* strain produced a sharp inhibition boundary, yielding a single, well-defined MIC (Fig. 1a and Supplementary Fig. 1a, b). This MIC was well below the clinical breakpoint for colistin (4 μg/mL), indicating that the wild-type (WT) ancestral strain is fully susceptible to colistin as expected.

To accelerate evolution, the DNA mismatch repair gene *mutS* was deleted—this deletion increases mutation rates by ~ 100-fold and is widely used in other evolutionary studies [19,20]. Deletion of *mutS* had no detectable effect on antibiotic susceptibility (Supplementary Fig. 1b, c). All genetic reconstruction conducted later used the WT background with an intact *mutS* gene.

Classical resistance evolves under continuous exposure

We first followed a conventional evolution protocol in which cells were exposed continuously to antibiotic, with selection pressure ratcheted upward by increasing antibiotic concentration over time (Fig. 1b; Methods) [21,22]. Etest and disk diffusion assays showed a uniformly reduced inhibition zone that was displaced toward higher antibiotic concentrations relative to the WT ancestor (Fig. 1a, c, d; Supplementary Fig. 1a), indicating the evolution of resistance. The inhibition boundary remained abrupt, yielding elevated yet well-defined MICs.

To quantify resistance, we performed population analysis profiling (PAP). Although labor-intensive, PAP measures cell survival as a function of antibiotic concentration, providing a direct readout of resistance frequency [3,23,24]. A PAP curve of final evolved clones exhibited uniformly high survival across increasing concentrations, followed by an abrupt drop to zero (Fig. 1e). This cutoff defines the MIC, which lies well above the clinical breakpoint (dashed line), thereby classifying the mutant as resistant. Importantly, this step-like profile indicates uniform survival up to a common threshold (i.e., MIC), revealing homogeneous resistance across the population.

Hereafter, we refer to this resistance type as mono-resistance (MR). This pattern agrees with the sharp inhibition boundaries observed in Etest and disk diffusion assays (Fig. 1c, d), explaining why these routine MIC-based diagnostics can robustly capture classical resistance.

To resolve the underlying evolutionary dynamics, we performed PAP on isolates sampled across multiple stages of evolution. Across successive cycles, PAP curves consistently displayed a step-like profile, while the entire curve shifted progressively rightward (Fig. 1i). This shift indicates a rising MIC and a population-wide increase in resistance, demonstrating the evolution of MR.

While continuous antibiotic exposure is commonly used to study resistance evolution, clinical antibiotic treatments are inherently dynamic [25]. Scheduled dosing (e.g., oral or intravenous administration at fixed intervals) generate repeated fluctuations in antibiotic concentration over time. We simulated this fluctuating antibiotic landscape by exposing *E. coli* to alternating cycles of colistin treatment for a period of T_{on} and colistin-free recovery for T_{off}. Previous studies have shown that cyclical regimens can increase antibiotic 'tolerance' [26-29], in which bacterial populations transiently halt growth to survive drug exposure. These studies were specifically designed to enrich tolerance by suddenly exposing stationary phase cells to very high drug concentrations (10 ~ 500 × MIC), thereby killing all actively growing cells. Such a procedure was chosen because tolerance is defined by a dormant state [30]. By contrast, resistance is defined by the ability of bacteria to continue growing in the presence of antibiotics [30]. We therefore maintained cultures in exponential phase throughout evolution experiments by serial dilution.

We first implemented intermittent exposure with equal treatment and recovery periods (T_{on}/T_{off} = 24/24 h, Supplementary Fig. 2a). Under these conditions, PAP curves again exhibited step-like profiles (Supplementary Fig. 2b). We then decreased T_{on} while extending T_{off} (12/36 h or 3/21 h, Supplementary Fig. 2a); yet PAP revealed the same step-like pattern (Supplementary Fig. 2a-d).

Thus, continuous antibiotic exposure or short fluctuations result in evolution of MR.

HR evolves under intermittent exposure with extended recovery periods

In clinical treatment settings, long antibiotic-free intervals can arise for multiple reasons, including non-adherence to prescribed regimens such as missed doses [31], infection relapse followed by repeated treatments [32] and transmission between hosts [33,34]. Thus, we further extended the antibiotic-free period in our experiments (T_{on}/T_{off} = 3/93 h), while keeping the total duration of the experiments similar to those above.

Under this regime, we observed a strikingly different evolutionary outcome. Etest and disk diffusion assays produced inhibition zones nearly indistinguishable from that of the susceptible ancestor, indicating that the MIC did not change (Fig. 1a, g, h; Supplementary Fig. 1a).

To quantify cell survival, we conducted PAP assay on the final evolved isolates. The PAP curve no longer exhibited a step-like profile in survival and instead showed a gradual decline with increasing drug concentration (Fig. 1e). Survival fell to very low levels at concentrations below the clinical breakpoint (dashed line), indicating that the majority of cells in the evolved strain remained susceptible, consistent with the minimal change in the primary inhibition zone in Etest and disk diffusion.

Yet the PAP curve also exhibited a long, low-frequency tail, indicating rare survivors at concentrations far above the apparent MIC: a hallmark of heteroresistance (HR). Motivated by this observation, we re-examined the Etest and disk diffusion plates and found a few small colonies within the primary inhibition zone in late-cycle isolates (Fig. 1h, inset; Supplementary Fig. 1a).

To quantitatively resolve how a susceptible WT strain evolves to become HR, we performed PAP

on isolates sampled across multiple stages, plotting survival frequency on a semi-log scale to resolve low-frequency survivors. Over successive cycles, survivors appeared at progressively higher colistin concentrations but at low frequencies, producing graded tails in the PAP curve (Fig. 1j). These tails widened over time, expanding the concentration range over which resistance was heterogeneous (Fig. 1j). This behavior contrasts sharply with MR, in which the PAP profile remained step-like throughout (Fig. 1i). Widely accepted operational criteria classify an isolate as HR if it contains subpopulations (frequency $\geq 10^{-6} – 10^{-7}$) capable of growth at $\geq 8\times$ the MIC of the main susceptible population [3,23,24]. By this definition, isolates recovered at Cycle 6 and thereafter classify as HR (Fig. 1j).

We next repeated the experiment using meropenem. The results mirrored those observed with colistin: continuous antibiotic exposure or short fluctuations selected for MR (Supplementary Fig. 3a-c), while intermittent exposure with long antibiotic-free recovery periods favored HR (Supplementary Fig. 3d, e).

HR emerges cryptically, reproducibly, and rapidly.

Notably, at the early stages (e.g., Cycle 6), this phenotype remains undetectable by Etest or disk diffusion, which yield inhibition boundaries identical to the susceptible ancestor and lacked obvious colonies within the zone (Fig. 1g; Supplementary Fig. 1a). Such colonies appeared only at later evolutionary cycles (Fig. 1h; Supplementary Fig. 1a). These comparisons highlight the cryptic emergence of HR, which is not readily captured by routine diagnostics.

Here, the PAP curves (Fig. 1i, 1j) were obtained by analyzing 50 independent colonies isolated from five parallel evolution cultures (10 colonies per culture). Importantly, each PAP curve was obtained from a single, purified clonal isolate; thus, the gradual decline in survival frequency

(Fig. 1j) reflects intrinsic phenotypic heterogeneity within a clonal population rather than a mixture of distinct genotypes. Furthermore, the close overlap among these 50 PAP curves (shaded regions, with symbols indicating the mean) indicates that HR evolution was consistent and reproducible.

We next analyzed the timescale of evolution. In the continuous and intermittent regimens above, one cycle spans 24 h and 96 h, respectively. We quantified evolutionary progress using $C_{\max}$, defined as the highest colistin concentration up to which survival was detectable in PAP. When $C_{\max}$ is plotted against elapsed time, it increases on comparable wall-clock time in the two regimes (Fig. 1k). However, the intermittent protocol applies colistin for only 3 of 96 h per cycle (a 1/32 drug duty cycle), whereas continuous exposure applies drug throughout. Accordingly, when $C_{\max}$ is plotted against cumulative time under antibiotic exposure, $C_{\max}$ increased >10-fold faster in HR than MR (Fig. 1l). Thus, for given antibiotic use, HR evolves substantially more efficiently than MR.

Single mutations are sufficient to generate HR.

The genetic mechanisms of classical resistance have been well studied [35]. By contrast, HR exhibits a distinct phenotypic pattern, raising the question of whether it requires complex genetic changes. Our experiments evolved mutants from a well-defined genetic background (*E. coli* K-12) and followed their lineages, providing a unique opportunity to identify genetic signatures that enable HR. We performed whole-genome sequencing of HR-evolved strains, identifying approximately 15 mutations that have accumulated over the course of evolution (Supplementary Fig. 4a). To assess their contributions, each mutation was introduced separately into the WT background. Most mutations had no detectable or only limited effects on colistin resistance

(Supplementary Fig. 4b). By contrast, two mutations—one in *pmrB* and one in *lpxC*—produced HR phenotypes (Fig. 2).

pmrB encodes the sensor kinase component of the PmrAB two-component regulatory system, which controls lipid A modification pathways. Sequencing revealed that HR was enabled by a missense mutation (C84Y; Fig. 2a), located within the N-terminal transmembrane/sensory region previously characterized for signal detection [36]. *lpxC* encodes an essential enzyme catalyzing the first committed step in lipid A biosynthesis. We found a two-residue deletion (ΔEY199–200, Fig. 2a) within a hydrophobic pocket implicated in substrate positioning, adjacent to the essential catalytic core [37].

Because transient gene amplification was proposed as a potential mechanism for HR [16], we examined copy-number variation in the evolved strains. Read-depth analysis occasionally yielded modestly elevated copy-number estimates (~2–3×) at a few isolated loci (Extended Data). This magnitude is far smaller than the previously reported amplifications (often tens- to hundreds-fold) [16,38]. Moreover, genes immediately adjacent to these loci retained baseline coverage (i.e., single-copy), lacking the contiguous multi-kilobase amplification structure expected for bona fide segmental duplication [16,39] (Extended Data). Together, these analyses argue against segmental amplification as the primary basis of HR in our evolved strains.

Importantly, introduction of either *pmrB* or *lpxC* mutation alone into the susceptible WT background was sufficient to convert the PAP profile to HR (Fig. 2b). The combined *pmrB* and *lpxC* mutations recapitulated the PAP shape of the evolved HR strain (Fig. 2b), indicating that these single mutations are key to enabling HR in our evolved lineages.

HR maintains its adaptive advantage through phenotypic partitioning and dynamic

enrichment

The rapid and reproducible emergence of HR in our evolution experiments suggests that HR confers a selective advantage. We sought to define this advantage and compare it with classical MR. This quantitative cost-benefit analysis is enabled by our experimental design, which yielded both MR and HR mutants with the same parental background, allowing direct, head-to-head fitness comparisons. We compared the fitness of MR and HR mutants from Cycle 24 and Cycle 10 respectively because they both are capable of growing in colistin up to the same maximal concentrations (C_{max}=16 μg/mL).

Given that the parent strain fails to grow at colistin concentrations above 0.25 μg/mL (Supplementary Fig. 1), the ability of MR and HR strains to survive up to 16 μg/mL, which is well above the clinical breakpoint 4 μg/mL, highlights the benefit of resistance. Yet this is accompanied by a cost; under antibiotic-free conditions, both MR and HR strains exhibited reduced growth rates relative to their susceptible ancestor (Supplementary Fig. 5a). By introducing the *pmrB*(C84Y) and *lpxC*(ΔEY199–200) mutations into WT (Fig. 2a), we found that these two mutations recapitulated the fitness cost of the HR strain (Supplementary Fig. 6).

However, when we directly compared the HR and MR strains, the former grew faster than the latter (Fig. 3a); see Supplementary Fig. 5a for their growth curves, and Supplementary Fig. 3f for meropenem-HR and MR. We additionally confirmed faster growth of HR than MR consistently throughout the evolution (Supplementary Fig. 5b and 3g). Thus, although resistance incurs a fitness cost, this cost is substantially lower in HR than in MR.

To understand the basis of HR's reduced fitness cost, we analyzed growth at single-cell resolution. The antibiotic responses of individual cells reveal heterogeneous phenotypes within

the HR population. Cells were first grown exponentially under antibiotic-free conditions (left of the arrow in Fig. 3b) and then exposed to colistin (arrow). Many cells were killed upon exposure to a colistin concentration (2 μg/mL; bottom panel, right of the arrow in Fig. 3b), indicating that they were susceptible. In contrast, a subset of cells continued to grow even after exposure to a high colistin concentration (16 μg/mL; top panel) and were classified as resistant.

After this classification, we quantified the antibiotic-free single-cell growth rate, λ_S, by analyzing the time-lapse trajectories prior to antibiotic exposure. This analysis revealed a clear fitness trade-off. In the absence of antibiotics, resistant cells grew slowly (Fig. 3b, c), with growth rates comparable to those of MR (Fig. 3a). In contrast, susceptible cells grew fast, forming larger microcolonies prior to exposure (Fig. 3b) and exhibiting higher growth rates (Fig. 3c). We observed the same cell-to-cell heterogeneity in antibiotic resistance and growth in the meropenem-evolved HR strain (Supplementary Fig. 7). Together, these results show that a HR population comprises phenotypic states with distinct growth–resistance trade-offs at the single-cell level.

We next analyzed how these phenotypes were managed in a population. Under antibiotic-free conditions, the fraction of resistant cells remains low (Supplementary Fig. 8a, b). Upon antibiotic exposure, this resistant subpopulation expands to comprise nearly the entire population, and then contracts back to its basal level once the antibiotic is removed (Supplementary Fig. 8a, b). This behavior contrasts sharply with MR, in which the resistant fraction remains fixed near 100% regardless of environmental conditions (Supplementary Fig. 8c, d).

Together, these observations indicate a dynamic strategy of HR: resistant phenotypes are transiently enriched during antibiotic exposure to ensure maximum survival, while susceptible, fast-growing cells dominate in antibiotic-free environments to maximize population growth. This

population-level restructuring of single-cell states provides a mechanistic basis for how HR achieves robust survival while maintaining a lower fitness cost of resistance.

Clinical isolates exhibit genetic and fitness signatures similar to laboratory-evolved strains

The analyses above establish a genetic basis and fitness advantage of HR in lab-evolved strains. To evaluate the clinical relevance of these findings, we next examined clinical isolates. Unlike our lab strains, which were derived from a single genetic background under defined exposure regimens, clinical isolates span diverse genetic backgrounds and unknown treatment histories. Despite this diversity, we discovered that their genetic and fitness signatures closely match those identified in our laboratory-evolved strains.

First, to compare genetic signatures, we surveyed prior clinical studies of colistin HR in the literature, primarily from Gram-negative ESKAPEE pathogens, including *Enterobacter* spp., *Escherichia coli*, *Klebsiella pneumoniae*, *Acinetobacter baumannii*, and *Pseudomonas aeruginosa* (see Supplementary Table 2). When we compiled the reported mutations, we found that genes in the *pmr* and *lpx* pathways were among the most frequently mutated loci (~50% and 15% respectively, Supplementary Fig. 9), consistent with the key mutations identified in our evolution experiments.

We next measured the fitness of clinical HR and MR isolates. We utilized the U.S. CDC Emerging Infections Program [9], analyzing a collection comprising primarily *Enterobacter*, *Escherichia*, and *Klebsiella* species. The population-level growth measurements showed that HR isolates consistently grow faster than MR isolates (Fig. 3a, right panel), indicating that a lower fitness cost of resistance is a robust feature of HR.

The microscopy analyses further revealed a similar phenotypic trade-off between growth and resistance at the single-cell level in clinical isolates (Supplementary Fig. 10). Moreover, the size of the resistant subpopulation in HR strains dynamically shifted in response to environmental conditions (Supplementary Fig. 8e, f), in contrast to a clinical MR isolate in which the resistant fraction remains fixed near 100% regardless of environment (Supplementary Fig. 8g, h).

Together, our results from clinical isolates and lab-evolved strains converge across genetic, fitness, and single-cell phenotypes. This convergence, despite diverse genetic backgrounds, suggests that comparable selective pressures operate in clinical settings, similar to those imposed in our evolution experiments. Importantly, our observation of HR's fitness advantage provides a mechanistic explanation for its widespread occurrence [3,7].

Fitness modeling recapitulates the distinct selective regimes underlying HR and MR

These findings raise an important question: why is HR not always favored over MR? Despite its adaptive advantage, HR has an inherent limitation: only a small minority of cells are initially resistant at the onset of antibiotic exposure. As a result, HR populations experience a substantial lag phase upon antibiotic exposure, until minority resistant cells expand sufficiently to support population growth (Fig. 3d). Such prolonged lag phases were observed in both laboratory-evolved strains (left panel) and clinical isolates (right panel).

Integrating these advantage and limitation into a mathematical framework, we sought to quantitatively explain the evolutionary conditions that favor HR. In our evolved HR populations, the frequency of cells surviving the highest colistin concentrations tested, C_{max}—that is, the resistant-subpopulation frequency (RF)—is typically ~0.01–0.1% of the total population (Fig. 1j), corresponding to an approximately 10^3–10^4-fold initial deficit upon antibiotic exposure. In

antibiotic-free conditions, however, HR populations grow faster than MR populations by ~0.1 h^{-1} (Fig. 3a).

We quantified this cost-benefit balance by calculating the geometric mean fitness over one cycle consisting of an antibiotic exposure period (T_{on}) followed by an antibiotic-free recovery period ($T_{recovery}$) (Supplementary Text). Eq. 7 gives the minimum recovery time required for HR to compensate for its initial deficit: $t \approx \frac{\ln(10^3-10^4)}{0.1} \approx 69\sim92$ hours, supporting our experimental finding that long recovery periods were required to evolve HR ($T_{recovery}$ = 93 h; Fig. 1f, j).

However, we have previously shown that the RF in clinical isolates can vary over several orders of magnitude [40]. Using Eq. 7, we therefore calculated the $T_{recovery}$ as a function of RF, yielding the diagonal dashed line in Fig. 4. This model reveals that the rarer the resistant subpopulation, the longer the recovery time required for its growth advantage in drug-free conditions to compensate for its deficit during treatment. Importantly, the dashed line defines the minimum $T_{recovery}$ needed for a given RF; HR is favored only above this boundary.

To compare this prediction with experiment, we mapped our colistin and meropenem evolution outcomes onto this phase diagram. We calculated the RFs by the number of survivors at C_{max}. Plotting the $T_{recovery}$ used in each experiment against this frequency places experimental points generally close, but above, the predicted minimum boundary (Fig. 4), supporting our model.

For practical interpretation, we overlaid standard operational classifications. At low frequencies ($\lesssim10^{-6}$–10^{-7}), resistant cells fall near the detection limit of PAP. In this regime, isolates are operationally treated as susceptible (S; green region in Fig. 4) [3,23,24]. At the opposite extreme, when a macroscopic fraction of the population is resistant (e.g., $\gtrsim$0.1–0.5), it is readily detected by routine assays and conventionally categorized as resistance (MR; blue region).

The intermediate regime corresponds to HR (red region). Importantly, this phase diagram shows that HR is favored only when recovery intervals are well above ~20 h (dotted line), with longer recovery intervals supporting lower resistant-subpopulation frequencies. These intervals are substantially longer than the within-day fluctuations generated by standard dosing schedules. However, such extended gaps can arise due to lapses in adherence including missed doses, which are known to occur commonly in outpatient settings [31].

Notably, the relevant timescale depends on fitness parameters. In our framework (Eq. 7), the minimum recovery time required for HR scales inversely with the antibiotic-free growth advantage of HR over MR ($\Delta\lambda$). In laboratory-evolved strains, we measured $\Delta\lambda \approx 0.1$ h^{-1} (Fig. 3a). In clinical isolates, the growth-rate advantage was approximately two-fold larger (Fig. 3a), which shifts the HR-favored boundary downward by roughly a factor of two. As a result, the recovery intervals required to favor HR can encroach upon within-day dosing timescales, indicating that we cannot completely rule out a contribution of standard dosing schedules to HR evolution.

Discussion

Evolution critically depends on history, yet the details of that history are often unknown, obscuring the adaptive origins of evolved traits [41]. In clinical settings, antibiotic landscapes are inherently complex, making it difficult to delineate evolutionary determinants. As a result, it has remained unclear when and how HR emerges and why it is so prevalent. Our study directly addresses this gap.

We show that HR evolves rapidly and reproducibly under treatment interruptions. Such interruptions are not unique to antibacterial therapy but also often arise in antifungal and

anticancer regimens [31,42], suggesting that similar selective pressures may operate in other systems.

This evolutionary pathway poses a particular clinical challenge. While resistance evolution may be unavoidable under sustained antibiotic selection, classical resistance (MR) is readily detectable by standard susceptibility testing, enabling rational therapeutic adjustment and stewardship responses. In contrast, we demonstrated that HR evolution is cryptic, obscuring both its emergence and its progression. Although we used PAP to detect HR, its labor-intensive and low-throughput nature limits routine clinical use [3]. Consequently, HR creates a diagnostic blind spot that constrains real-time epidemiological surveillance and permits treatment failure to occur without a clear warning signal.

Why does such diagnostically elusive resistance emerge? Our fitness analyses provide a mechanistic explanation. By generating phenotypic heterogeneity, a HR population minimizes the fitness costs associated with resistance during drug-free intervals. Upon antibiotic exposure, rare resistant cells enable population survival. Their frequency dynamically shifts, decreasing to low levels in antibiotic-free conditions. Thus, the cryptic nature of HR is not directly selected per se; instead, it arises as a byproduct of the adaptive population structure. Once established, the low fitness burden of HR facilitates its maintenance, providing a mechanistic explanation for its widespread occurrence.

Figure Captions

Fig. 1. De novo evolution of heteroresistance (HR).

(a) Representative inhibition-zone image of WT *E. coli* ancestral strain. See Supplementary Fig. 1 for corresponding disk diffusion and PAP curve.

(b) Schematic of the continuous-treatment regimen. One cycle consisted of 24 hours of treatment. In each cycle, cultures were exposed to both 0.5× and 1× MIC. When growth was observed at the latter, the antibiotic concentration was increased two-fold in the subsequent cycle.

(c, d) Representative inhibition-zone images of mutants evolved under continuous selection. Mutants from Cycle 16 (c) and 30 (d) were shown. Clear inhibition boundaries progressively shift inward, consistent with increasing resistance. Disk diffusion assays show similar shifts (Supplementary Fig. 1a).

(e) Population analysis profiling (PAP) curves of a WT (green color), the MR mutant (blue color) and HR mutant (red color). Final evolved strains (Cycle 30 for MR and 14 for HR) were analyzed. The MR strain maintains high survival across increasing drug concentrations, while the HR strain exhibits a gradual decline with a long high-concentration tail, reflecting survival of resistant minorities. The dashed line indicates the colistin clinical breakpoint (4 μg/ml). Three biological replicates (symbols) were tested; black lines and error bars denote mean ± s.d.

(f) Schematic of the alternating-treatment regimen. Each cycle consisted of 3 h of colistin exposure followed by 93 h drug-free recovery (total cycle length = 96 h).

(g, h) Representative inhibition-zone images of mutants evolved under alternating exposure. Mutants from Cycle 6 (g) and Cycle 14 (h) are shown. The primary inhibition boundary remains largely unchanged. At later stages, small colonies appear within the inhibition zone (insets).

(i, j) Evolutionary trajectories resolved by PAP across cycles. (i) Under continuous exposure, PAP curves shift uniformly rightward while retaining a sharp cutoff, consistent with population-wide increases in resistance (MR). (j) Under alternating exposure, PAP curves progressively

develop a graded high-concentration tail, indicating expansion of increasingly resistant but progressively rarer subpopulations (HR). PAP curves are plotted on a semi-log scale to visualize low-frequency survivors. Solid dots represent the mean survival frequency of independent colonies (n=50) from five parallel cultures; shaded regions indicate the full range.

(k, l) Kinetics of resistance acquisition. Maximum resistant concentration, $C_{\max}$, as a function of wall-clock time (k) and cumulative time spent in drug (l), highlighting more rapid emergence of HR per unit drug exposure compared to MR. Symbols denote three replicate populations; lines connect individual data points where shown.

Fig. 2. Genetic analysis of evolved HR strains.

(a) Colistin-evolved HR strains were analyzed by whole-genome sequencing (Supplementary Fig. 4a). Each mutation identified was introduced individually into a WT background using CRISPR-assisted λ-Red recombination (Supplementary Fig. 4b), identifying two critical mutations — the *pmrB*(C84Y) and *lpxC*(ΔEY199–200).

(b) Introduction of either *pmrB*(C84Y) or *lpxC*(ΔEY199–200) into WT was sufficient to produce HR phenotypes. Combining these two mutations recapitulated the PAP profile of the evolved HR strain (Cycle 14). Survival frequency is shown on a log scale. Different symbols represent independent replicate cultures (n = 5); Lines and error bars indicate their mean and standard deviation.

Fig. 3. Fitness analysis of HR and MR.

(a) Left panel: Growth rates (λ) of evolved strains. The MR strain from Cycle 24 and HR strain from Cycle 10 was characterized. Different symbols represent independent replicate cultures (n = 5). Right panel: Growth rate of clinical isolates collected through the CDC's Multi-site Gram-

negative Surveillance Initiative (MuGSI) [9]. The dataset includes colistin-MR (n = 5) and HR (n = 18) isolates. All isolates belong to the *Enterobacterales* order and comprise predominantly *Enterobacter*, *Escherichia*, and *Klebsiella* species. Species identities and individual growth rates are provided in Source Data.

(b) Time-lapse microscopy of an evolved colistin-HR strain. Images to the left of the arrow show the pre-treatment phase; those to the right show the post-treatment phase. Cells were classified based on their response to colistin post-treatment: resistant (surviving at 16 μg/mL) or susceptible (killed at 2 μg/mL). Scale bar: 10 μm.

(c) At single-cell level, susceptible cells exhibited significantly higher growth rates prior to colistin exposure. Three independent experiments were conducted, with 50 cells per group per replicate.

(d) Lag times of lab-evolved strains (left panel, n = 5) and clinical isolates (right panel, sample sizes were n = 5 for MR and 18 for HR) after exposure to antibiotic at 0.5× the strain-specific MIC.

Black lines and error bars indicate the mean and standard deviation. ***$p < 0.001$, based on one-way ANOVA with multiple comparisons.

Fig. 4. Phase diagram predicting when HR is evolutionarily viable.

The dashed line (Eq. 7) indicates the minimum $T_{recovery}$ required for a population with a given resistant-subpopulation frequency to emerge. Shaded regions denote operational classifications of susceptibility (S), HR, and MR. The red region indicates the HR regime. Black circles (colistin) and squares (meropenem) show experimental evolution outcomes across distinct

schedules; error bars indicate standard deviation. Experimental points lie close to, but above, the predicted boundary, supporting the model.

Methods

Bacterial strains and culture conditions

Escherichia coli K-12 strain NCM3722 (referred to as NMK1) was used. A Δ*mutS* derivative of NMK1 (designated NMK476) was constructed via P1 transduction from the Keio collection. *Enterobacter cloacae* clinical isolates were collected through the Georgia Emerging Infections Program, as part of the CDC's Multi-site Gram-negative Surveillance Initiative (MuGSI) in Georgia, USA.

Luria Broth (LB; Fisher Scientific #BP1426500) and LB agar (Fisher Scientific #BP1425500) were used for cell culturing. 5mL of cultures were incubated in test tubes with shaking at 250 rpm at 37 °C. OD_{600} readings were taken every 20–35 minutes using a Genesys20 spectrophotometer.

Antibiotics

Colistin sulfate (#1264-72-8) was obtained from Sigma-Aldrich. Meropenem trihydrate (#119478-56-7) was obtained from Research Product Industry. Ampicillin (#69-52-3), kanamycin sulfate (#70560-51-9) and chloramphenicol (#56-75-7) were purchased from Bio Basic.

Experimental evolution assays

Experimental evolution assays were conducted using NCM3722 Δ*mutS* (NMK476). A single colony was picked from an LB agar plate (previously streaked from -80°C glycerol stocks) and cultured overnight for 16 hours in LB broth with shaking at 250 rpm.

Continuous exposure: Overnight cultures were diluted into fresh LB medium containing either 0.5× MIC (e.g., 0.25 µg/mL) or 1× MIC (e.g., 0.5 µg/mL) of an antibiotic to a starting OD_{600} of 0.01. Cultures were incubated at 37 °C with constant shaking for 24 hours (one cycle). Bacterial growth was assessed visually and/or by measuring OD_{600}. If growth was observed only in the 0.5× MIC condition, cultures were again diluted into fresh 0.5× and 1× MIC media, and the cycle was repeated. Once growth was detected in the 1× MIC condition, this culture was diluted into LB medium containing 1× and 2× MIC concentrations (e.g., 0.5 and 1 µg/mL). This stepwise two-fold increase in drug concentration continued every 24 hours, with cultures passaged to higher concentrations only after successful growth at the latter concentration. Throughout the experiments, cultures were diluted into fresh LB with drug at OD_{600} = 0.01 every 12 hours.

Alternation of antibiotic and antibiotic-free phases: We first conducted treatment cycles of 24 hours of antibiotic exposure and 24 hours of antibiotic-free phase (24 hr on/24 h/off). Cultures were initially diluted from overnight growth into fresh LB containing 0.5× MIC (e.g., 0.25 µg/mL) and 1× MIC (0.5 µg/mL) of an antibiotic at a starting OD_{600} of 0.01 and incubated at 37 °C with shaking for 24 hours. If growth occurred only in the 0.5× MIC condition, cultures from this condition were washed twice with fresh LB to remove residual antibiotic, then transferred into drug-free LB at an OD_{600} of 0.001 and incubated for 24 hours. Cultures were then diluted back into fresh LB containing 0.5× and 1× MIC drug concentrations at OD_{600} = 0.01, and the cycle was repeated.

Once growth was observed in the 1× MIC tube, cells from that culture were again washed, transferred to drug-free LB at OD_{600} = 0.001, incubated for 24 hours, and exposed to 1× and 2× MIC. These alternating cycles were repeated with stepwise increases in drug concentration.

We tested different cycling periods 24 h on / 24 h off, 12 h on/ 36 off, 3 h on/ 21 h off, and 3 h on/ 93 h off of colistin treatment (Fig. 1b, f, Supplementary Fig. 2a), and 24 h on / 24 h off, 12 h on/ 36 h off and 6 h on/ 42 h off of meropenem treatment (Supplementary Fig. 3a, d). During drug-free phases, cultures were diluted into fresh LB at OD_{600} = 0.001 every 12 hours.

Population analysis profile (PAP) tests

The PAP assay enumerates colony-forming units (CFU) on plates containing increasing drug levels. During evolution experiments, cultures were streaked on agar plates. Single colonies were resuspended in LB broth to OD_{600} ~ 0.1, and serially diluted in LB in a 96-well plate (Corning #3598). 5 μL from each dilution was plated on LB agar containing antibiotics at indicated concentrations. CFU on drug-containing plates normalized by CFU on drug-free plates (after 24 hours of incubation) was calculated to determine resistance frequency.

Etest and disk diffusion

Bacterial cultures were harvested during exponential phase, centrifuged at 8000 × g for 3 min, and resuspended in 1× PBS. Cell suspensions were adjusted to 0.5 McFarland standard. Sterile cotton swabs were dipped into the cell suspension and then used to evenly swab the surface of Mueller–Hinton agar plates. For Etest, colistin MIC test strips (0.016–256 μg/mL) (Liofilchem™ #921411) were placed according to the manufacturer's instructions. For disk diffusion, sterile 6-mm disks were loaded with 64 μg of colistin sulfate and applied to the agar surface. Plates were incubated at 37 °C for 18–20 h and imaged after incubation.

Whole-genome sequencing

Genomic DNA was extracted using the QIAamp DNA Mini Kit (Qiagen #51304) according to the manufacturer's instructions. Purified DNA samples were submitted to SeqCenter (Pittsburgh, PA, USA) for whole-genome sequencing and bioinformatic analysis.

Strain construction: genome editing

A CRISPR-assisted λ-Red recombination system [43] was used to introduce precise mutations into the genome of wild-type *E.coli* NCM3722 (NMK1). The λ-Red recombinase (expressed by pKD46) and CRISPR-Cas9 system were co-utilized to promote homology-directed repair at the targeted genomic site. A 20-bp spacer (listed in Supplementary Table 3) was cloned into the CRISPR plasmid (pCRISPR) using BsaI digestion and T4 DNA ligase.

Electrocompetent NMK1 cells carrying pKD46 (NMK99) were prepared by growing cultures at 30 °C to an OD_{600} of 0.2–0.3, inducing λ-Red expression with 0.2% L-arabinose, and washing cells sequentially with ice-cold water and 10% glycerol.

For co-electroporation, 50 µL of electrocompetent cells were mixed with 100 ng each of pCas9 and pCRISPR::spacer plasmids, along with 200 pmol of single-stranded DNA repair template (60 nt) (listed in Supplementary Table 3). Electroporation was performed at 1.8 kV, 25 µF, and 200 Ω, followed by recovery in SOC medium at 37 °C for 2 h. Transformants were selected on LB agar containing ampicillin (100 µg/mL), kanamycin (50 µg/mL), and chloramphenicol (25 µg/mL), and incubated at 30 °C overnight.

Genomic DNA from selected colonies was isolated, and the targeted region (~300 bp flanking the mutation site) was amplified by PCR and verified via Sanger sequencing to confirm the

desired mutation. For plasmid curing, verified mutants were propagated without antibiotics and incubated at 42 °C to eliminate the temperature-sensitive pKD46.

Microscopy

Cultures grown to OD_{600} ~0.1 were placed on a 35 mm glass-bottom dish (Cellvis) and covered with a 1.5% LB-agarose gel pad. Imaging was performed using an Olympus IX83 inverted microscope equipped with a 60× oil immersion phase-contrast objective within a pre-warmed (37 °C) incubation chamber (InVivo Scientific).

Time-lapse imaging of cells for growth rate determination was performed over a 2-hour period with an interval time of 10 minutes before exposure to colistin or meropenem. To assess the viability of growth-rate tracked cells, imaging was continued every 30 minutes following application of 2 µg/mL or 16 µg/mL colistin or meropenem to the gel pad.

Images were segmented and cell area was measured using the MicrobeJ plugin for Fiji/ImageJ (version 5.13 I). Growth rates were calculated from areal changes in 150 cells per subpopulation.

Statistical analyses

Statistical analysis was conducted using GraphPad Prism. Details of biological replicates and statistical tests are provided in the corresponding figure legends. All data sets were tested for normality using the Shapiro-Wilk test and were confirmed to meet the normality criteria. Statistical analyses were performed as appropriate based on the experimental design.

Acknowledgements

This work was funded by NIH (1U19AI158080, MM, MK). We thank David Weiss, Dan Andersson, Bruce Levin and Daniel Weissman for helpful discussions throughout the projects.

Author Contributions.

MM and MK conceived the study. MM designed and carried out the experiments and analyzed the data. MK secured funding and provided resources. MM and MK wrote the manuscript. All authors read and approved the manuscript.

Competing Interests

Authors declare no competing interests.

Data Availability Statements

Source data for figures are provided in the Source Data file.

Reference

1 Davies, J. & Davies, D. Origins and evolution of antibiotic resistance. *Microbiology and molecular biology reviews : MMBR* **74**, 417-433 (2010). https://doi.org/10.1128/MMBR.00016-10

2 Kowalska-Krochmal, B. & Dudek-Wicher, R. The Minimum Inhibitory Concentration of Antibiotics: Methods, Interpretation, Clinical Relevance. *Pathogens* **10** (2021). https://doi.org/10.3390/pathogens10020165

3 Andersson, D. I., Nicoloff, H. & Hjort, K. Mechanisms and clinical relevance of bacterial heteroresistance. *Nature Reviews Microbiology* **17**, 479-496 (2019). https://doi.org/10.1038/s41579-019-0218-1

4 Band, V. I. & Weiss, D. S. Heteroresistance: A cause of unexplained antibiotic treatment failure? *PLoS pathogens* **15**, e1007726 (2019). https://doi.org/10.1371/journal.ppat.1007726

5 Alexander, H. E. & Leidy, G. MODE OF ACTION OF STREPTOMYCIN ON TYPE b HEMOPHILUS INFLUENZAE : II. NATURE OF RESISTANT VARIANTS. *J Exp Med* **85**, 607-621 (1947). https://doi.org/10.1084/jem.85.6.607

6 Paine, T. F. & Finland, M. Streptomycin-sensitive, -dependent, and -resistant Bacteria. *Science* **107**, 143-144 (1948). https://doi.org/doi:10.1126/science.107.2771.143

7 Roch, M., Sierra, R. & Andrey, D. O. Antibiotic heteroresistance in ESKAPE pathogens, from bench to bedside. *Clinical microbiology and infection : the official publication of the European Society of Clinical Microbiology and Infectious Diseases* **29**, 320-325 (2023). https://doi.org/10.1016/j.cmi.2022.10.018

8 Band, V. I. & Weiss, D. S. Heteroresistance to beta-lactam antibiotics may often be a stage in the progression to antibiotic resistance. *PLOS Biology* **19**, e3001346 (2021). https://doi.org/10.1371/journal.pbio.3001346

9 Band, V. I. *et al.* Colistin Heteroresistance Is Largely Undetected among Carbapenem-Resistant Enterobacterales in the United States. *mBio* **12**, e02881-02820 (2021). https://doi.org/doi:10.1128/mBio.02881-20

10 Dagogo-Jack, I. & Shaw, A. T. Tumour heterogeneity and resistance to cancer therapies. *Nat Rev Clin Oncol* **15**, 81-94 (2018). https://doi.org/10.1038/nrclinonc.2017.166

11 Zhai, B. *et al.* Antifungal heteroresistance causes prophylaxis failure and facilitates breakthrough Candida parapsilosis infections. *Nature Medicine* **30**, 3163-3172 (2024). https://doi.org/10.1038/s41591-024-03183-4

12 Beaumont, H. J. E., Gallie, J., Kost, C., Ferguson, G. C. & Rainey, P. B. Experimental evolution of bet hedging. *Nature* **462**, 90 (2009). https://doi.org/10.1038/nature08504

13 Gallie, J. *et al.* Bistability in a Metabolic Network Underpins the De Novo Evolution of Colony Switching in Pseudomonas fluorescens. *PLOS Biology* **13**, e1002109 (2015). https://doi.org/10.1371/journal.pbio.1002109

14 Rainey, P. B. *et al.* The evolutionary emergence of stochastic phenotype switching in bacteria. *Microbial cell factories* **10**, S14 (2011). https://doi.org/10.1186/1475-2859-10-S1-S14

15 Morawska, L. P., Hernandez-Valdes, J. A. & Kuipers, O. P. Diversity of bet-hedging strategies in microbial communities—Recent cases and insights. *WIREs Mechanisms of Disease* **14**, e1544 (2022). https://doi.org/https://doi.org/10.1002/wsbm.1544

16 Nicoloff, H., Hjort, K., Levin, B. R. & Andersson, D. I. The high prevalence of antibiotic heteroresistance in pathogenic bacteria is mainly caused by gene amplification. *Nature Microbiology* **4**, 504-514 (2019). https://doi.org/10.1038/s41564-018-0342-0

17 Band, V. I. *et al.* Antibiotic failure mediated by a resistant subpopulation in Enterobacter cloacae. *Nature Microbiology* **1**, 16053 (2016). https://doi.org/10.1038/nmicrobiol.2016.53

18 Gajic, I. *et al.* Antimicrobial Susceptibility Testing: A Comprehensive Review of Currently Used Methods. *Antibiotics (Basel)* **11** (2022). https://doi.org/10.3390/antibiotics11040427

19 Wei, W. *et al.* Rapid evolution of mutation rate and spectrum in response to environmental and population-genetic challenges. *Nature communications* **13**, 4752 (2022). https://doi.org/10.1038/s41467-022-32353-6

20 Swings, T. *et al.* Adaptive tuning of mutation rates allows fast response to lethal stress in Escherichia coli. *eLife* **6**, e22939 (2017). https://doi.org/10.7554/eLife.22939

21 Maeda, T. & Furusawa, C. Laboratory Evolution of Antimicrobial Resistance in Bacteria to Develop Rational Treatment Strategies. *Antibiotics (Basel)* **13** (2024). https://doi.org/10.3390/antibiotics13010094

22 Toprak, E. *et al.* Evolutionary paths to antibiotic resistance under dynamically sustained drug selection. *Nature Genetics* **44**, 101-105 (2012). https://doi.org/10.1038/ng.1034

23 Band, V. I. *et al.* Antibiotic combinations that exploit heteroresistance to multiple drugs effectively control infection. *Nat Microbiol* **4**, 1627-1635 (2019). https://doi.org/10.1038/s41564-019-0480-z

24 El-Halfawy, O. M. & Valvano, M. A. Antimicrobial Heteroresistance: an Emerging Field in Need of Clarity. *Clinical Microbiology Reviews* **28**, 191-207 (2015). https://doi.org/10.1128/cmr.00058-14

25 Roberts, J. A. *et al.* DALI: defining antibiotic levels in intensive care unit patients: are current β-lactam antibiotic doses sufficient for critically ill patients? *Clinical infectious diseases : an official publication of the Infectious Diseases Society of America* **58**, 1072-1083 (2014). https://doi.org/10.1093/cid/ciu027

26 Fridman, O., Goldberg, A., Ronin, I., Shoresh, N. & Balaban, N. Q. Optimization of lag time underlies antibiotic tolerance in evolved bacterial populations. *Nature* **513**, 418-421 (2014). https://doi.org/10.1038/nature13469

27 Mechler, L. *et al.* A Novel Point Mutation Promotes Growth Phase-Dependent Daptomycin Tolerance in Staphylococcus aureus. *Antimicrob. Agents Chemother.* **59**, 5366-5376 (2015). https://doi.org/doi:10.1128/aac.00643-15

28 Van den Bergh, B. *et al.* Frequency of antibiotic application drives rapid evolutionary adaptation of Escherichia coli persistence. *Nature Microbiology* **1**, 16020 (2016). https://doi.org/10.1038/nmicrobiol.2016.20

29 Bizzini, A. *et al.* A Single Mutation in Enzyme I of the Sugar Phosphotransferase System Confers Penicillin Tolerance to Streptococcus gordonii. *Antimicrob. Agents Chemother.* **54**, 259-266 (2010). https://doi.org/doi:10.1128/aac.00699-09

30 Balaban, N. Q. *et al.* Definitions and guidelines for research on antibiotic persistence. *Nature Reviews Microbiology* **17**, 441-448 (2019). https://doi.org/10.1038/s41579-019-0196-3

31 Osterberg, L. & Blaschke, T. Adherence to Medication. *New England Journal of Medicine* **353**, 487-497 (2005). https://doi.org/doi:10.1056/NEJMra050100

32 Figueroa, I. *et al.* Relapse versus reinfection: recurrent Clostridium difficile infection following treatment with fidaxomicin or vancomycin. *Clinical infectious diseases : an official publication of the Infectious Diseases Society of America* **55 Suppl 2**, S104-109 (2012). https://doi.org/10.1093/cid/cis357

33 van Bunnik, B. A. *et al.* Small distances can keep bacteria at bay for days. *Proceedings of the National Academy of Sciences of the United States of America* **111**, 3556-3560 (2014). https://doi.org/10.1073/pnas.1310043111

34 Vasquez, K. S. *et al.* Quantifying rapid bacterial evolution and transmission within the mouse intestine. *Cell Host Microbe* **29**, 1454-1468.e1454 (2021). https://doi.org/10.1016/j.chom.2021.08.003

35 Munita, J. M. & Arias, C. A. Mechanisms of Antibiotic Resistance. *Microbiol Spectr* **4** (2016). https://doi.org/10.1128/microbiolspec.VMBF-0016-2015

669 36 Gao, R. & Stock, A. M. Biological insights from structures of two-component proteins.
670 *Annual review of microbiology* **63**, 133-154 (2009).
671 https://doi.org/10.1146/annurev.micro.091208.073214

672 37 Whittington, D. A., Rusche, K. M., Shin, H., Fierke, C. A. & Christianson, D. W. Crystal
673 structure of LpxC, a zinc-dependent deacetylase essential for endotoxin biosynthesis.
674 *Proceedings of the National Academy of Sciences of the United States of America* **100**,
675 8146-8150 (2003). https://doi.org/10.1073/pnas.1432990100

676 38 Pereira, C., Larsson, J., Hjort, K., Elf, J. & Andersson, D. I. The highly dynamic nature of
677 bacterial heteroresistance impairs its clinical detection. *Communications Biology* **4**, 521
678 (2021). https://doi.org/10.1038/s42003-021-02052-x

679 39 Slack, A., Thornton, P. C., Magner, D. B., Rosenberg, S. M. & Hastings, P. J. On the
680 Mechanism of Gene Amplification Induced under Stress in Escherichia coli. *PLoS*
681 *genetics* **2**, e48 (2006). https://doi.org/10.1371/journal.pgen.0020048

682 40 Ma, M. & Kim, M. High-resolution, high-throughput detection of hidden antibiotic
683 resistance with the dilution-and-delay (DnD) susceptibility assay. *Nature communications*
684 (2026). https://doi.org/10.1038/s41467-026-70174-z

685 41 Gould, S. J. & Lewontin, R. C. The spandrels of San Marco and the Panglossian
686 paradigm: a critique of the adaptationist programme. *Proc R Soc Lond B Biol Sci* **205**,
687 581-598 (1979). https://doi.org/10.1098/rspb.1979.0086

688 42 Robin DiMatteo, M., Giordani, P. J., Lepper, H. S. & Croghan, T. W. Patient Adherence
689 and Medical Treatment Outcomes: A Meta-Analysis. *Medical Care* **40** (2002).

690 43 Jiang, W., Bikard, D., Cox, D., Zhang, F. & Marraffini, L. A. RNA-guided editing of
691 bacterial genomes using CRISPR-Cas systems. *Nature Biotechnology* **31**, 233-239
692 (2013). https://doi.org/10.1038/nbt.2508

693

Figure 1

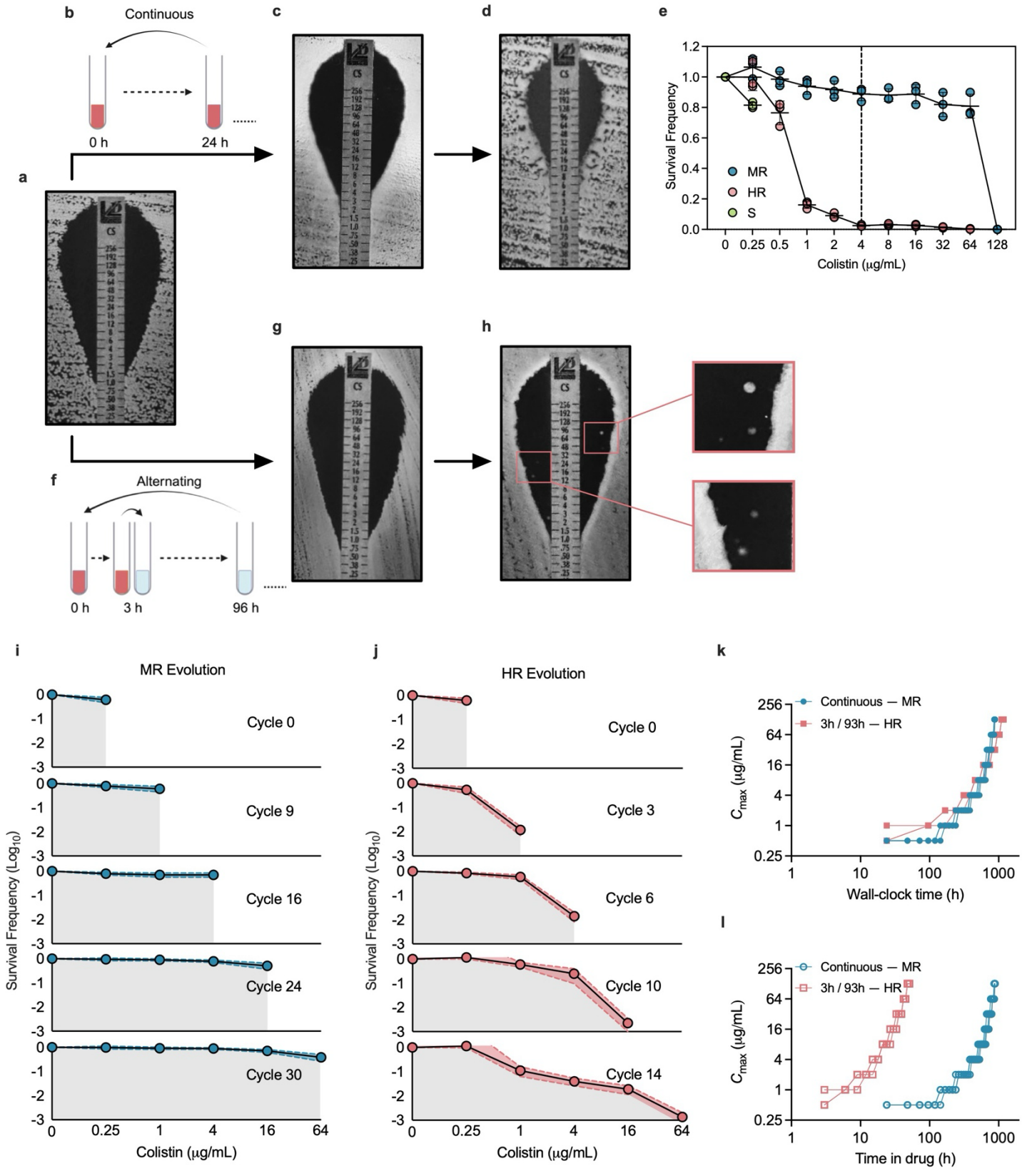
a
b
Continuous
0 h
24 h
c
d
e
Survival Frequency
MR
HR
S
Colistin (μg/mL)
f
Alternating
0 h
3 h
96 h
g
h
i
MR Evolution
Cycle 0
Cycle 9
Cycle 16
Cycle 24
Cycle 30
Survival Frequency (Log10)
Colistin (μg/mL)
j
HR Evolution
Cycle 0
Cycle 3
Cycle 6
Cycle 10
Cycle 14
k
Continuous — MR
3h / 93h — HR
Cmax (μg/mL)
Wall-clock time (h)
l
Time in drug (h)

Figure 2

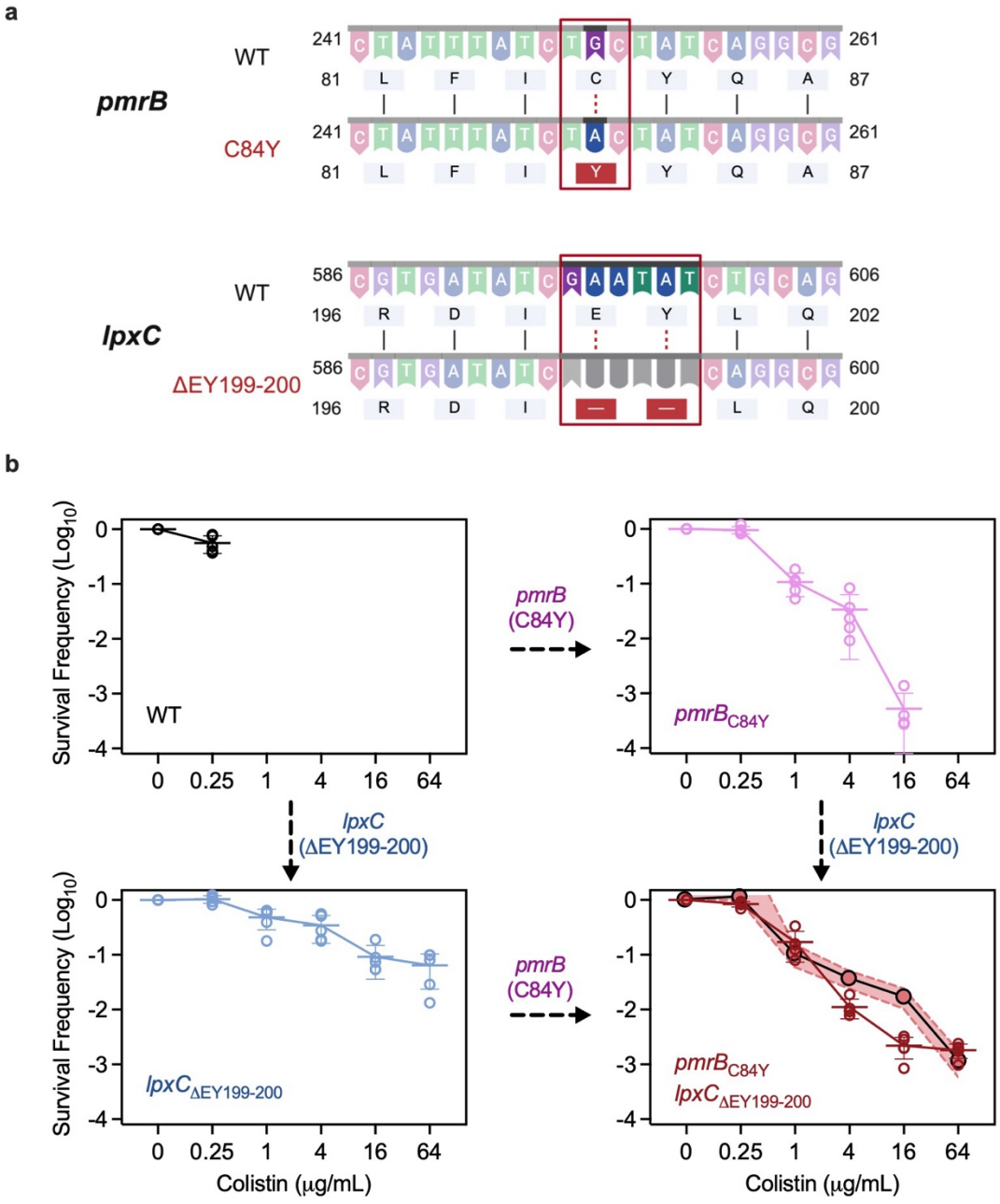
a
pmrB
WT
C84Y
241 C T A T T T A T C T G C T A T C A G G C G 261
81 L F I C Y Q A 87
241 C T A T T T A T C T A C T A T C A G G C G 261
81 L F I Y Y Q A 87
lpxC
WT
ΔEY199-200
586 C G T G A T A T C G A A T A T C T G C A G 606
196 R D I E Y L Q 202
586 C G T G A T A T C C A G G C G 600
196 R D I — — L Q 200
b
Survival Frequency (Log10)
0 -1 -2 -3 -4
WT
pmrB (C84Y)
pmrBC84Y
lpxC (ΔEY199-200)
lpxCΔEY199-200
pmrB (C84Y)
pmrBC84Y
lpxCΔEY199-200
0 0.25 1 4 16 64
Colistin (μg/mL)

Figure 3

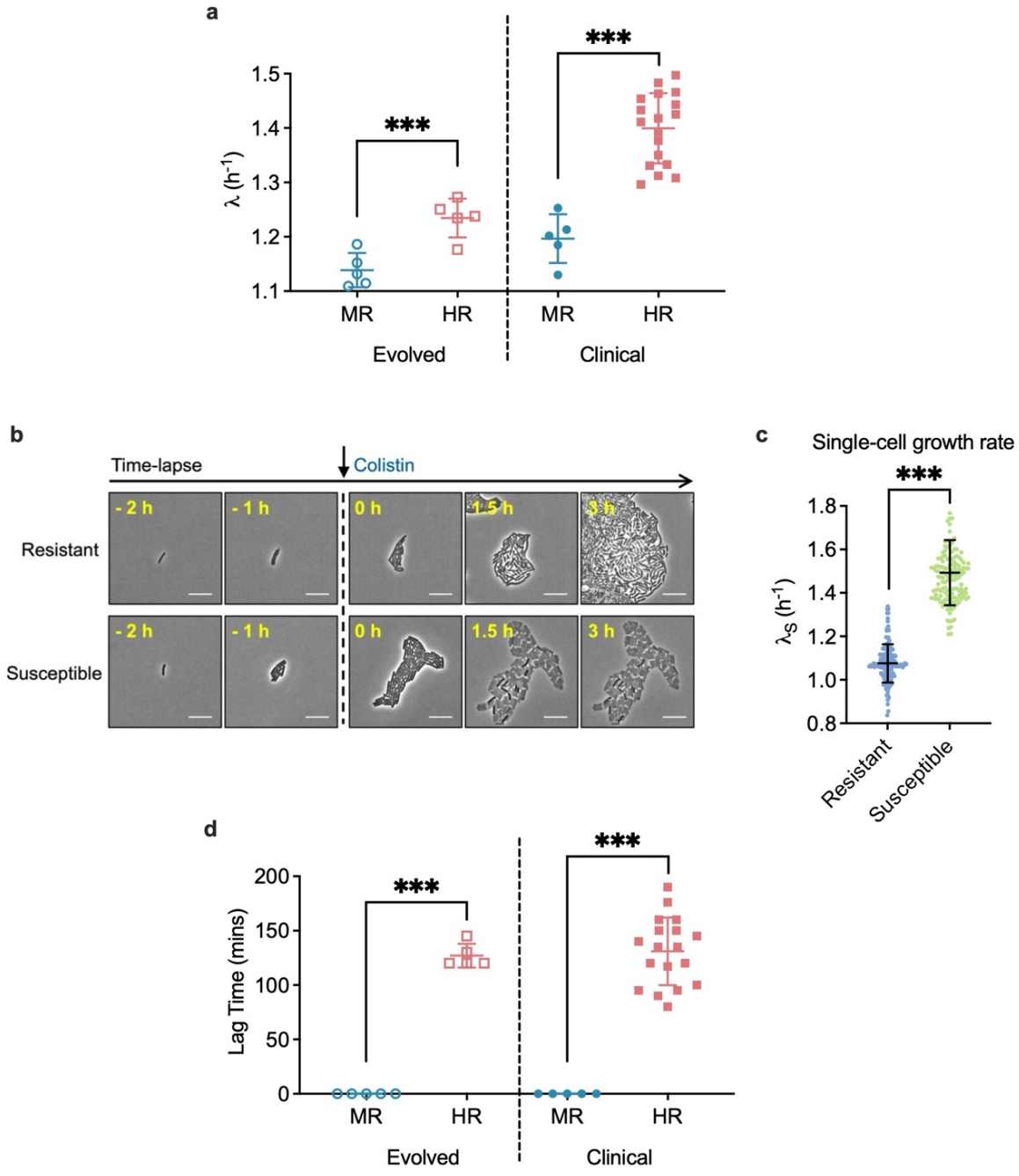
a
***
***
λ (h-1)
1.5
1.4
1.3
1.2
1.1
MR
HR
MR
HR
Evolved
Clinical
b
Time-lapse
Colistin
Resistant
Susceptible
- 2 h
- 1 h
0 h
1.5 h
3 h
c
Single-cell growth rate
***
λS (h-1)
1.8
1.6
1.4
1.2
1.0
0.8
Resistant
Susceptible
d
***
***
Lag Time (mins)
200
150
100
50
0
MR
HR
MR
HR
Evolved
Clinical

Figure 4

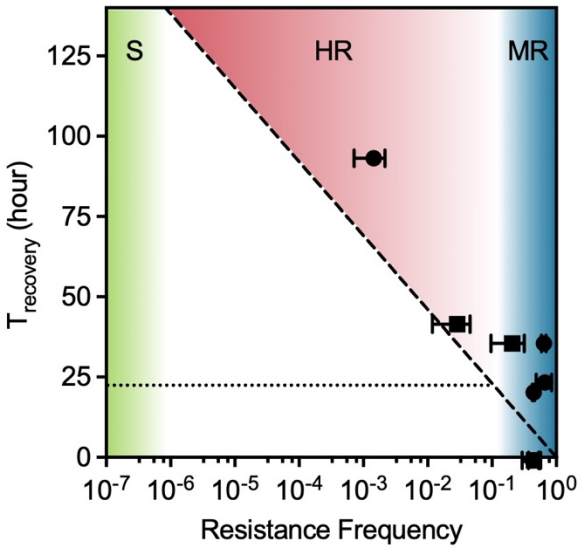
S
HR
MR
125
100
75
50
25
0
$T_{recovery}$ (hour)
10^{-7} 10^{-6} 10^{-5} 10^{-4} 10^{-3} 10^{-2} 10^{-1} 10^{0}
Resistance Frequency